Analytical and Bioanalytical Chemistry
https://doi.org/10.1007/s00216-018-1501-0

RESEARCH PAPER

A novel magnetic fluorescent biosensor based on graphene quantum dots for rapid, efficient, and sensitive separation and detection of circulating tumor cells

Fangchao Cui[1] · Jian Ji[1] · Jiadi Sun[1] · Jun Wang[2] · Haiming Wang[4] · Yinzhi Zhang[1] · Hong Ding[3] · Yong Lu[3] · Dan Xu[5] · Xiulan Sun[1]

Received: 15 August 2018 / Revised: 8 November 2018 / Accepted: 16 November 2018

Abstract

We describe a "turn-on" magnetic fluorescent biosensor based on graphene quantum dots (GQDs), Fe_3O_4, and molybdenum disulfide (MoS_2) nanosheets. It is used for rapid, efficient, and sensitive separation and detection of circulating tumor cells (CTCs). A facile approach (electrochemical synthesis method) for the preparation of photoluminescent GQDs functionalized with an aptamer [epithelial cell adhesion molecule (EpCAM) receptors] and a magnetic agent for one-step bioimaging and enrichment of CTCs is described. MoS_2 nanosheets, as a fluorescence quencher, and the aforementioned aptamer@Fe_3O_4@GQD complex were assembled to construct "turn-on" biosensing magnetic fluorescent nanocomposites (MFNs). This system exhibits low cytotoxicity and an average capture efficiency of 90%, which is higher than that of other magnetic nanoparticles on account of the one-step CTC separation method. In addition, the MFNs could quickly identify and label CTCs within 15 min, surpassing other one-step and two-step marker detection methods. Furthermore, because of the presence of aptamers, the MFNs have specific capability to capture CTCs (both low- and high-EpCAM-expressing cells). In addition, high-sensitivity detection of up to ten tumor cells in whole blood was achieved. Therefore, the MFNs have great potential to be used as universal biosensing nanocomposites for fluorescence-guided tumor cell enrichment and bioimaging.

Keywords Graphene quantum dots · Aptamer · Circulating tumor cells · Magnetic fluorescence biosensor · Magnetic separation

Fangchao Cui and Jian Ji contributed equally to this work.

Electronic supplementary material The online version of this article (https://doi.org/10.1007/s00216-018-1501-0) contains supplementary material, which is available to authorized users.

✉ Xiulan Sun
sxlzyz@jiangnan.edu.cn

[1] School of Food Science, State Key Laboratory of Food Science and Technology, National Engineering Research Center for Functional Foods, School of Food Science Synergetic Innovation Center of Food Safety and Nutrition, Jiangnan University, Wuxi 214122, Jiangsu, China

[2] Department of Toxicology, Key Laboratory of Modern Toxicology (NJMU), Ministry of Education, School of Public Health, Nanjing Medical University, Nanjing 211166, Jiangsu, China

[3] National Institutes for Food and Drug Control, Beijing 100050, China

[4] Guangzhou GRG Metrology & Test Co. Ltd, Guangzhou 510000, Guangdong, China

[5] School of Food and Biological Engineering, Shaanxi University of Science and Technology, Xi'an 710021, Shaanxi, China

Introduction

Cancer is among the leading causes of death worldwide, trailing only heart disease in incidence. Promising approaches to significantly improve survival of cancer patients include detecting tumors at an early stage before they have the chance to grow larger or metastasize, as well as improving tumor resection through identification of cancerous tissues [1, 2]. Typically, most cancer-related deaths are caused by metastatic disease [3]. Some of this metastasis is caused by the shedding of circulating tumor cells (CTCs) into the blood circulation, although the probability of metastasis is not high [4]. CTCs in the blood of healthy people are almost undetectable, but the detection rate in blood in many cancer patients is extremely high [5]. Especially in the early stages of cancer, typically 1–100 CTCs are detected per 10^9 blood cells [6]. Therefore, quantitative detection of CTCs can result in early diagnosis of cancer, whether metastasis, and postoperative monitoring. Currently, the CellSearch system is unique medical equipment

Published online: 05 January 2019

approved by the US Food and Drug Administration for clinical CTC testing [5]. However, the technique requires expensive equipment, is time-consuming, and requires antibody staining, limiting widespread application of the technology [7].

The criteria for classic CTC staining comprise the existence of cell-surface epithelial cell adhesion molecule (EpCAM) and cytoplasmic epithelial keratin, as well as the lack of hematopoietic CD45 markers [5], EpCAM is the most frequently studied tumor-associated antigen because it is overexpressed in most types of cancer, including colorectal cancer, breast cancer, pancreatic cancer, and liver cancer [5, 8–11]. EpCAM is used as a biomarker to diagnose cancer and for prognosis of cancer [12]. However, most EpCAM-based diagnostic and therapeutic methods rely on the use of an anti-EpCAM antibody, since the antibody in a physiological environment of large size and instability can induce an objective clinical response [13]. The aptamer is small, is easy to synthesize, has good stability, can penetrate tissues quickly, has good biocompatibility, and is gradually becoming an excellent substitute for antibodies [14].

Fluorometric assays with inherent advantages of low background noise and high sensitivity are considered to be more ideal methods for bioassays [15, 16]. Graphene quantum dots (GQDs) have been studied for fluorescence imaging. Compared with traditional imaging materials, including organic dyes, fluorescent proteins easily photobleach and are chemically unstable, limiting their application. New fluorescent nanoparticles, such as quantum dots [17] and upconversion nanoparticles [18], are photostable fluorescent probes but their biological applications are limited by their high toxicity. GQDs as a fluorescent probe completely solve these problems. GQDs have the advantages of stable photoluminescence (PL), low cytotoxicity, excellent biocompatibility, and resistance to photobleaching [19–21]. GQDs have been found to be safe for both in vitro and in vivo use [22–25]. Driven by these important features, GQDs are more widely used in biomedical imaging and labeling probes [26, 27].

Herein we report novel nitrogen and sulfur doped GQDs (N,S/GQDs) constructed by a facile approach. The resulting GQDs emit bright and stable blue luminescence in solution under single-wavelength UV excitation (λ= 340 nm). A novel aptamer@Fe_3O_4@GQD@MoS_2-based nanosurface energy transfer (NSET) assay using the aptamer@Fe_3O_4@GQD complexes as donors and MoS_2 nanosheets as quenchers was developed for the detection of EpCAM. The NSET method developed is well suited for detecting EpCAM. Its linear detection range is 2–64 nM, and the limit of detection (LOD) is 1.19 nM. Because of the presence of aptamers, this nanobiosensor can quickly (15 min) identify and detect tumor cells (both low- and high-EpCAM-expressing cells). In addition, because of the presence of Fe_3O_4, the captured cells can be easily separated for further accurate analysis.

Materials and methods

Materials

High-purity graphite rods were purchased from Shanghai Carbon Co. (Shanghai, China). MoS_2 nanosheets and Fe_3O_4 modified with amino groups were purchased from Nanjing Mknano Science and Technology Co. (Nanjing, Jiangsu, China). Sodium *p*-toluenesulfonate (TsONa), 1-ethyl-3-(3-dimethylaminopropyl)carbodiimide (EDC), and *N*-hydroxysulfosuccinimide (NHS) were purchased from Sigma-Aldrich (St Louis, MO, USA). All solvents and reagents were purchased from Aladdin Industrial Corporation (Shanghai, China). The aptamer was synthesized and purified by Sangon Biotech Co. (Shanghai, China). A 48-base hairpin-structured aptamer modified with a carboxyl group (5′-/5carboxyl/-CAC TAC AGA GGT TGC GTC TGT CCC ACG TTG TCA TGG GGG GTT GGC CTG-3′) was used as the probe [28]. EpCAM recombinant human protein (hIgG1-FcTa), purchased from Sino Biological (North Wales, PA, USA), was used as the EpCAM-positive protein target. Stock solutions of the aptamer and protein were prepared in ultrapure water.

Preparation of N,S/GQDs

The N,S/GQDs were prepared by an electrochemical method in accordance with a previous report [29]. The N,S/GQDs were synthesized by electrolysis of graphite rods in 0.1 M TsONa and acetonitrile solution at a potential of +3.0 V. The electrolysis of the graphite rods was performed with a CHI 660B electrochemical workstation with the current intensity in the range from 80 to 120 mA cm^{-2}. After a 2-h electrochemical reaction, the reactant was filtered through a 0.22-μm membrane filter to remove the precipitated graphite oxide and graphite particles. The N,S/GQDs were further purified by ultrafiltration (Amicon Ultra-0.5, 30 kDa; Millipore, Billerica, MA, USA) to remove the large GQDs, and the lower solution was collected. The resulting N,S/GQD solution was dialyzed against deionized water in a dialysis bag (3500 Da) for 1 day, with the deionized water changed every 8 h. Ultimately, the as-prepared N,S/GQDs were stored at 4 °C for further characterization and use.

Characterization of the N,S/GQDs

Transmission electron microscopy (TEM) analysis was conducted with a JEM 2100 instrument (JEOL, Tokyo, Japan). Atomic force microscopy (AFM) images were captured with a MultiMode V scanning probe microscope (Veeco Instruments, Plainview, NY, USA). Fourier transform infrared (FTIR) spectra were recorded with a Spectrum 100 FTIR spectrometer (PerkinElmer, Waltham, MA, USA). X-ray

photoelectron spectroscopy (XPS) analysis was conducted with an ESCAlab 250Xi electron spectrometer from Thermo Scientific (Waltham, MA, USA) with 300-W Al Kα radiation. The base pressure was about 3×10^{-9} mbar. The binding energies were referenced to the C 1*s* line at 284.8 eV from adventitious carbon. The UV–vis absorption and PL spectra were measured with a UV-2450 spectrometer and a Cary Eclipse fluorimeter (SHIMADZU Ltd., Tokyo, Japan), respectively. Excitation and emission spectra were measured with an FLS920P instrument (Edinburgh Instruments, Livingston, UK). Confocal optical micrographs were captured with a confocal laser scanning microscope (Leica SP8, Nikon, Japan).

Synthesis of aptamer-conjugated amino-functionalized Fe_3O_4

The carboxyl-modified aptamer was covalently conjugated to the amino-functionalized Fe_3O_4 by the EDC and *N*-hydroxysuccinimide (NHS) method. Initially, the carboxyl-modified aptamer was pretreated with EDC and NHS for 15 min. Subsequently, the activated aptamer at a final concentration of 1.95 μM was added to the amino-functionalized Fe_3O_4 solution. The mixture was then shaken overnight at room temperature. To remove excessive EDC, NHS, and aptamer, the final product, the Fe_3O_4@aptamer complex, was purified and concentrated by ultrafiltration (Amicon Ultra-0.5, 30 kDa, Millipore).

Preparation of aptamer@Fe_3O_4@GQD nanoparticles

Briefly, 2.4 mg EDC and 3.6 mg *N*-hydroxysulfosuccinimide were added to 1 mL carboxylated GQD solution (1 mg/mL), and the mixture was stirred for 15 min. Then, 1 mL Fe_3O_4@aptamer complex was added, and the mixture was incubated with activated GQD-COOH overnight at room temperature. Finally, the aptamer@Fe_3O_4@GQD nanoparticle solution was purified and concentrated by ultrafiltration (Amicon Ultra-0.5, 30 kDa, Millipore).

NSET assay establishment and EpCAM detection

The NSET quenching efficiency and EpCAM detection were recorded with an FLSP920 spectrophotometer (Edinburgh instruments Ltd., UK) equipped with a 450-W steady-state xenon lamp at room temperature. In a typical experiment, the final product of aptamer@Fe_3O_4@GQD complexes (10 mL) was incubated with MoS_2 nanosheets (10 mL) with a series of final MoS_2 concentrations ranging from 50 to 500 mg/mL. After 20 min incubation, the sample was measured with the excitation and emission wavelengths set at 340 and 450 nm, respectively. For EpCAM detection, the aptamer@Fe_3O_4@GQD@MoS_2 nanocomplexes were incubated with an increasing concentration of target protein (2, 4, 8, 16, 32, and 64 nM). After 2 h incubation at 37 °C in the dark, the fluorescence signal for each concentration of the target protein was measured. Control experiments were conducted by our measuring the fluorescence signal of the sample after addition of the same volume of phosphate-buffered saline (PBS) instead of the target protein. All the fluorescence spectra were recorded under the same conditions.

Cell culture

EpCAM-overexpressing hepatocellular carcinoma (Hep G2), low-EpCAM-expressing lung cancer A549 (ATCC CCL-185; non-small-cell lung cancer), and EpCAM-nonexpressing HEK293 cell lines were obtained from American Type Culture Collection (Manassas, VA, USA). Cells were grown in Dulbecco's modified Eagle's medium supplemented with 10% fetal bovine serum and 1% penicillin and streptomycin in a humidified atmosphere containing 5% CO_2 at 37 °C.

Cell labeling by aptamer@Fe_3O_4@GQD complexes

Hep G2, A549, and HEK293 cells were plated at a density of 10^5 cells per square centimeter, and were allowed to adhere by incubation for 12 h at 37 °C. To evaluate the specificity of the aptamer@Fe_3O_4@GQD@MoS_2 nanoprobes for Hep G2 and A549 cells, aptamer@Fe_3O_4@GQD@MoS_2 complexes (0.2 mg/mL) and GQDs (0.2 mg/mL) were separately added to 500 μL Dulbecco's modified Eagle's medium. Then the nanomaterials were incubated with tumor cells for 15 min, 2 h, and 6 h. Subsequently, the cells were washed to remove the nanomaterials and then observed under a confocal microscope (405-nm excitation light). The PL intensity of each sample was analyzed with the software program ZEN (Carl Zeiss, Oberkochen, Germany).

Detection of tumor cells and cell capture efficiency

For tumor cell detection, 0, 10, 50, 100, 200, and 300 Hep G2 and A549 cells were added to 10^6 HEK293 cells in 500 μL PBS and incubated with aptamer@Fe_3O_4@GQD@MoS_2 complexes (0.2 mg/mL) at 37 °C for 15 min. Subsequently, the cells were centrifuged and washed to remove excess nanoparticles. Then the cells were resuspended in 500 mL PBS and separated with a magnet in a 1.5-mL tube. Eventually, the cells obtained were resuspended in 100 mL PBS and imaged under a confocal microscope. To study the capture efficiency, 10, 30, 100, 200, and 300 Hep G2 cells in 500 μL PBS were prepared and labeled with aptamer@Fe_3O_4@GQD complexes. After magnetic separation, the number of tumor cells captured in the samples is determined based on the calculation of fluorescence intensity.

For the detection of tumor cells in blood, we added the desired numbers of Hep G2 cells (0, 10, 30, 100, and 1000) to 500 μL of whole blood. The cell labeling, magnetic

separation, and detection were performed following the same procedure as described earlier.

Results and discussion

Mechanism of the nanoprobe-based NSET sensing system

The sensing mechanism of the aptamer@Fe_3O_4@GQD@MoS_2-based NSET biosensor for detection of CTCs is depicted in Fig. 1. GQDs emit blue light at 450 nm under excitation with 340-nm UV light and can be used as the NSET donor. Two-dimensional MoS_2 nanosheets can be used as the NSET acceptor for sensing platforms because of their good quenching ability. Carboxylated GQDs were first synthesized by electrolysis of graphite rods in a solution of 0.1 M TsONa in ultrapure water at a potential of +3.0 V for 2 h, followed by dialysis against deionized water and ultrafiltration with a 30-kDa Amicon filter. The carboxylated aptamer was conjugated to the amino-functionalized Fe_3O_4 by the EDC and NHS method. Then carboxylated GQDs were also conjugated to the amino-functionalized Fe_3O_4 by the EDC and NHS method. The sensing platform uses van der Waals forces to adsorb aptamers on MoS_2 nanosheets, which results in close proximity of GQDs and MoS_2. Because of the ultrahigh annihilation capability of MoS_2, the PL signal of GQDs is highly quenched by MoS_2 with 340-nm excitation. When EpCAM on the surface of the CTC membrane appears, the powerful binding affinity between the aptamer@Fe_3O_4@GQD complex and EpCAM can separate the aptamer@Fe_3O_4@GQD complex from the MoS_2 nanosheets, resulting in the recovery of the fluorescence signal. The change in the fluorescence signal was used to detect the target CTCs. Some of the EpCAM@aptamer@Fe_3O_4@GQD complexes were ingested by CTCs, which can be separated from normal cells by magnetic separation because of the presence of Fe_3O_4.

Synthesis and characterization of the fluorescence and physical and chemical properties of N,S/GQDs

N,S/GQDs were synthesized by electrolysis of graphite rods in a solution of 0.1 M TsONa in water at a potential of +10.0 V for 4 h, followed by dialysis against deionized water, purification by ultrafiltration (30-kDa filter), and collection of the lower solution with the smaller particles. The resulting GQDs dissolved in deionized water to form clear solutions. The UV–vis absorption spectrum of N,S/GQDs is displayed in Fig. 2a. The π–π* transition of the graphite sp^2 domain results in a typical absorption peak at 270 nm. An n–π* absorption band at approximately 310 nm was also observed. Unlike other reported GQD studies, the PL peak of the sample does not shift as the excitation wavelength changes. The PL of N,S/GQDs was detected before and after purification (Fig. S1) and then compared for different pH values (Fig. S2). The findings

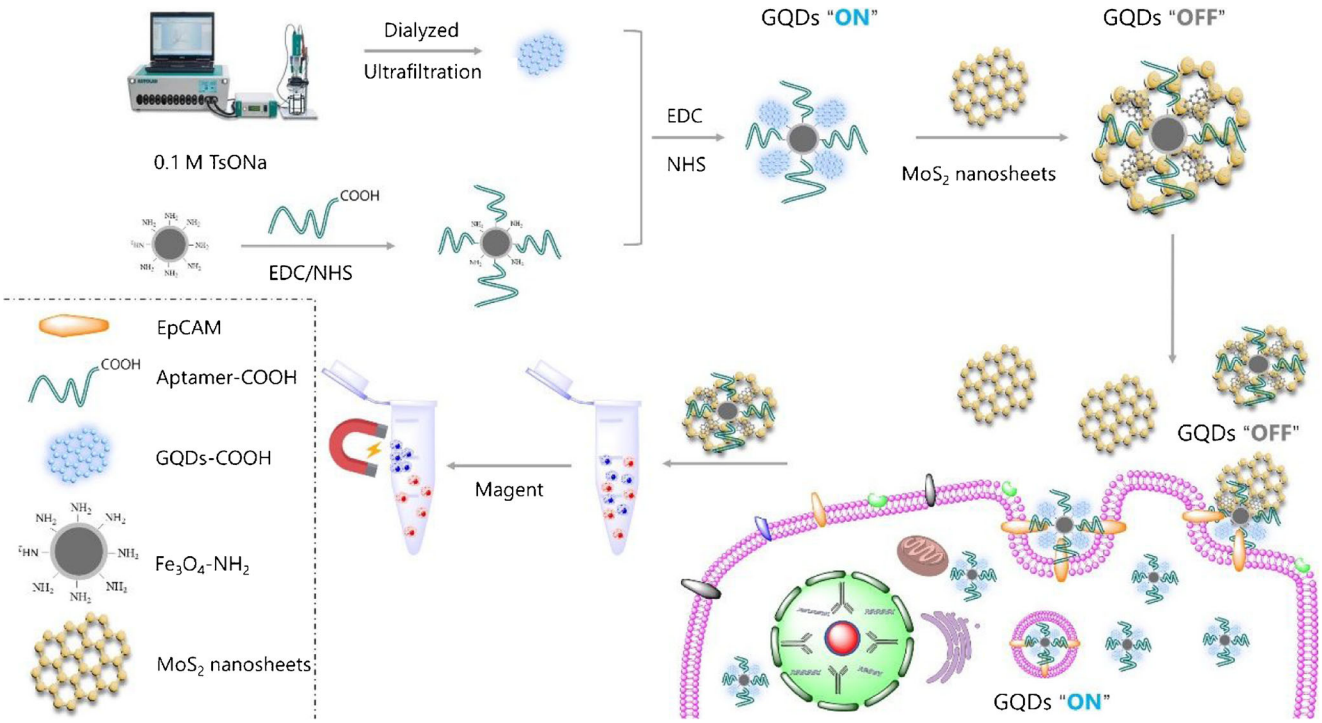

Fig. 1 The sensing mechanism of the aptamer@Fe_3O_4@graphene quantum dot (GQD)@MoS_2-based nanosurface energy transfer biosensor for the detection of circulating tumor cells (CTCs). EDC 1-ethyl-3-(3-dimethylaminopropyl)carbodiimide, EpCAM epithelial cell adhesion molecule, NHS *N*-hydroxysuccinimide, TsONa sodium *p*-toluenesulfonate

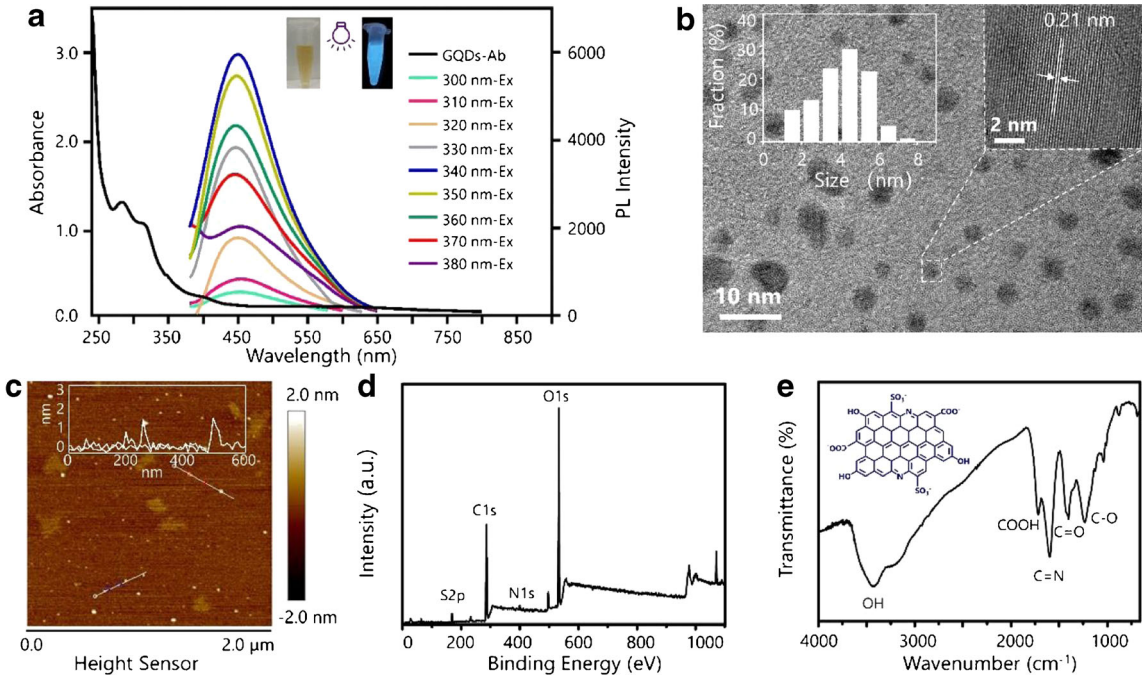

Fig. 2 Characterization of the fluorescence and physical and chemical properties of N,S/graphene quantum dots (GQDs). **a** UV–vis absorption spectrum, photoluminescence spectra, and images (inset) in daylight (left) and under UV irradiation at 365 nm (right) of N,S/GQDs at different excitation wavelengths. **b** Size distribution (left inset), transmission electron microscopy (TEM) image, and high-resolution TEM image (right inset) of N,S/GQDs. **c** Height distribution (inset) and atomic force microscopy image of N,S/GQDs. **d** X-ray photoelectron spectroscopy analysis of N,S/GQDs. **e** Fourier transform IR spectrum and proposed structure (inset) of N,S/GQDs. Ab antibody

confirmed the consistency of the optical properties of our samples. The optical homogeneity of our samples led to a thorough study of the luminescence mechanism of GQDs' composition and structure. When diverse ions were introduced, the PL intensity of GQDs did not change significantly (see Fig. S10). This result indicates that most metal and salt ions (concentration of 0.1 M) have no effect on the PL properties of GQDs.

TEM analysis (Fig. 2b) and AFM analysis (Fig. 2c) revealed that the N,S/GQDs have uniform size, with an average diameter of approximately 5 nm (Figs. 2b and S3) and a topographic height of 1.8 nm (Fig. 2c, inset). Additionally, the high-resolution TEM images displayed in the insets illustrate that the N,S/GQDs have well-resolved lattice fringes (0.21-nm pitch). This is consistent with the (100) in-plane lattice of graphene (Fig. 2b), indicating that many N,S/GQDs consist of approximately one to three graphene layers [30]. The results of the TEM and AFM analysis were consistent with previous results for the optical homogeneity of GQDs. The XPS analysis results suggested that N,S/GQDs are composed of carbon (28.91%), nitrogen (5.44%), sulfur (3.08%), and oxygen (62.57%) (Fig. 2d). The high-resolution C 1*s* spectrum exhibited a main peak at 284.3 eV, which confirms the graphite structure (sp^2 C–C). The peaks at 285.6, 286.2, 287.0, and 288.0 eV suggest the presence of C–S, C–N, C–O, and C=O, respectively (Fig. S4a). The high-resolution N 1*s* spectrum indicated the existence of pyridinic nitrogen (399.7 eV) (Fig. S4b). The high-resolution S 2*p* spectrum indicated the existence of –C–SO_x– (x = 2, 3, 4) (Fig. S4c). The FTIR spectra illustrated in Fig. 2e reveal that N,S/GQDs have abundant hydrophilic groups, such as O–H (3425 cm^{-1}), C=O (1258 cm^{-1}), and COOH (1759 cm^{-1}), on the surface, guaranteeing their good dispersity in water [31]. Furthermore, telescopic vibrations of C=N (1642 cm^{-1}) and C–O (1258 cm^{-1}) bonds were observed in N,S/GQDs, indicating that polyaromatic structures were present in the N,S/GQDs [32]. On the basis of these findings, we hypothesized that the structure of N,S/GQDs includes carboxyl, hydroxy, C=N, and C–SO_3^- groups (Fig. 2e).

Construction and characterization of the aptamer@Fe_3O_4@GQD complexes

To successfully construct aptamer@Fe_3O_4@GQD complexes, aptamer@Fe_3O_4 complexes were first synthesized and then the GQDs were coupled to them. UV–vis spectra of the nanocomponents were recorded (Fig. 3a). GQDs and the aptamer displayed absorption peaks at 310 and 280 nm, respectively. No obvious absorption peak of Fe_3O_4 nanoparticles was observed. After GQDs had been conjugated to aptamer@Fe_3O_4 complexes, characteristic peaks at 280 and 310 nm were observed, indicating the formation of aptamer@Fe_3O_4@GQD complexes.

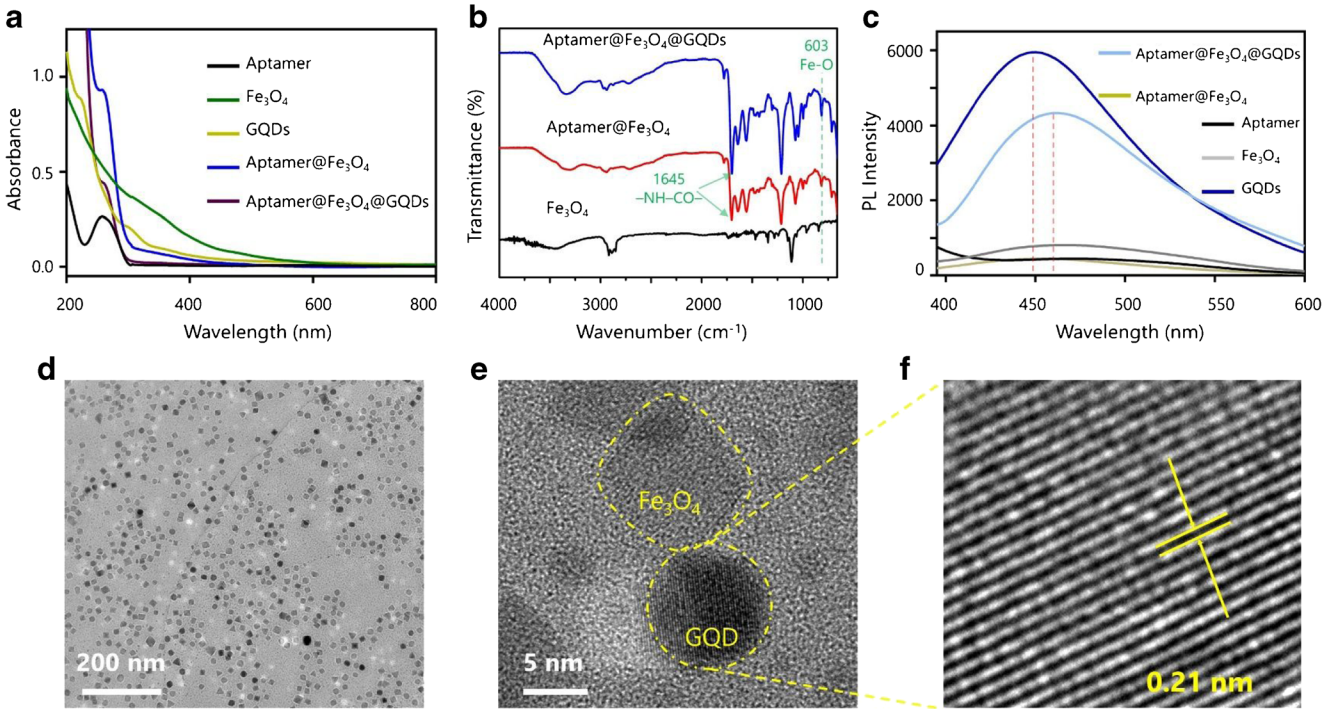

Fig. 3 Construction and characterization of the aptamer@Fe_3O_4@graphene quantum dot (GQD) complex. **a** UV–vis spectra of the aptamer, Fe_3O_4, GQDs, aptamer@Fe_3O_4 complex, and aptamer@Fe_3O_4@GQD complex. **b** Fourier transform IR spectra of the aptamer@Fe_3O_4@GQD complex, aptamer@Fe_3O_4 complex, and Fe_3O_4. **c** Photoluminescence (PL) spectra of the aptamer, Fe_3O_4, GQDs, aptamer@Fe_3O_4 complex, and aptamer@Fe_3O_4@GQD complex. **d** Transmission electron microscopy (TEM) image of bare Fe_3O_4 nanoparticles. **e** TEM image of aptamer@Fe_3O_4@GQD nanoparticles. **f** High-resolution TEM image of a GQD.

The FTIR spectra of aptamer@Fe_3O_4@GQD complexes, aptamer@Fe_3O_4 complexes, and Fe_3O_4 were also recorded (Fig. 3b). Magnetic Fe_3O_4 nanoparticles have a characteristic Fe–O peak (603 cm^{-1}). Further, –OH bending and stretching vibrations appear in the FTIR spectrum (at approximately 3450 cm^{-1}). Since both the aptamer and the GQDs have a carboxyl group and Fe_3O_4 was amino-functionalized, after the aptamer is covalently bound, the new peak in the 1645-cm^{-1} is attributable to the vibration of –NH–CO–. This finding reveals that an amide bond is formed in the aptamer@Fe_3O_4 complex. The peak height of that chemical bond was increased after covalent binding to GQDs.

Additionally, under 340-nm UV excitation, GQDs and aptamer@Fe_3O_4@GQD complexes emitted blue light. The peak emission from 447 nm (GQDs) to 459 nm (aptamer@Fe_3O_4@GQD complexes) has a very small offset emission peak of GQDs after ultrafiltration with a 30-kDa filter (Fig. 3c). For Fe_3O_4, aptamer, and aptamer@Fe_3O_4 complex, no obvious emission peak was observed in the spectra, which indicated successful construction of aptamer@Fe_3O_4@GQD complexes.

To further characterize the formation of aptamer@Fe_3O_4@GQD complexes, TEM analysis was used to characterize the form and size of Fe_3O_4 and aptamer@Fe_3O_4@GQD complexes. The average size of the Fe_3O_4 nanoparticles was around 12 nm (Fig. 3d). Binding of GQDs to the aptamer@Fe_3O_4 complex via an amide bond allows GQDs to attach to the surface of the aptamer@Fe_3O_4 complex (Fig. 3e). Moreover, high-resolution TEM images revealed that the GQDs had a lattice fringe with a spacing of around 0.21 nm (Fig. 2f), which also indicated the successful construction of aptamer@Fe_3O_4@GQD complexes.

Establishment of an NSET system based on the aptamer@Fe_3O_4@GQD complex and MoS_2 nanosheets

The UV–vis spectra of MoS_2 (Fig. S8a) show an absorption peak at 285 nm. The surface of MoS_2 nanosheets was negatively charged and the zeta potential was about -38 mV (Fig. S5 and Table S1). The graphene-like two-dimensional structure of MoS_2 nanosheets (Fig. S8b) makes them over the internet nanosensing biomolecules having a high load factor. The average size of MoS_2 nanosheets is about 375nm. A TEM image of the aptamer@Fe_3O_4@GQD@MoS_2 composites is shown in Fig. S8c. Figure S8d (magnified high-resolution TEM image) clearly illustrates that MoS_2 nanosheets have a good adsorption effect on the aptamer@Fe_3O_4@GQD complex. The optimal emission spectrum of the aptamer@Fe_3O_4@GQD complexes excited at 340 nm exhibits blue luminescence at 460 nm (Fig. S8a). The establishment of the NSET system between the aptamer@Fe_3O_4@GQD complex and MoS_2 nanosheets benefited from the overlap between the emission spectrum of the aptamer@Fe_3O_4@GQD complexes and the absorption spectrum of MoS_2 nanosheets. The images (Fig. S8a, inset) of the

nanoparticles before (left) and after (right) addition of the MoS_2 nanosheets indicated that the PL signal of GQDs was quenched because of energy transfer from GQDs to MoS_2 nanosheets.

Establishment of the aptamer@Fe_3O_4@GQD@MoS_2 -based NSET biosensor and detection of EpCAM

Optimization of the ratio of donor and acceptor molecules is important for the development of NSET methods with high quenching efficiency. Five milliliters of 1 mg/mL aptamer@Fe_3O_4@GQD solution (donor) was incubated with an equal volume of 50–500 μg/mL MoS_2 nanosheet solution (acceptor). We thereby obtained the optimum ratio of the aptamer@Fe_3O_4@GQD complex and the MoS_2 nanosheets, and the maximum quenching efficiency. The PL signal of the aptamer@Fe_3O_4@GQD@MoS_2 nanocomposite was then measured for a series of ratios (donor-to-acceptor ratios from 100 to 2.5). The control is the PL intensity of the aptamer@Fe_3O_4@GQD solution mixed with an equal volume of ultrapure water. The PL spectra and images (under 365-nm UV irradiation) of the aptamer@Fe_3O_4@GQD@MoS_2 composite for different ratios are illustrated in Fig. 4a. The results showed that the PL signal of aptamer@Fe_3O_4@GQD complexes was negatively correlated with the concentration of the added MoS_2 nanosheets. When the concentration is increased from 50 to 500 μg/mL, the PL intensity gradually decreases. The aptamer@Fe_3O_4@GQD complexes adsorbed onto the MoS_2 nanosheets and fluorescence quenching was induced. The adsorption resulted in the GQDs being close enough to the MoS_2 nanosheets to cause energy transfer. We used the following equation for the energy transfer efficiency:

$$\text{Quenching efficiency} = \left(F_0 - F_q\right)/F_0$$

where F_0 represents the original PL signal of the control and F_q is the PL intensity of the aptamer@Fe_3O_4@GQD complexes after quenching by the MoS_2 nanosheet. Figure 4b shows the calculated PL signal quenching efficiency and the normalized PL intensity. The proportion of the donor in the recipient reaches 2.5, the maximum PL signal quenching efficiency is 91.2%, and the minimum normalized PL intensity (F_q/F_0) is 8.7%. This proves that MoS_2 nanosheets have excellent fluorescence quenching ability.

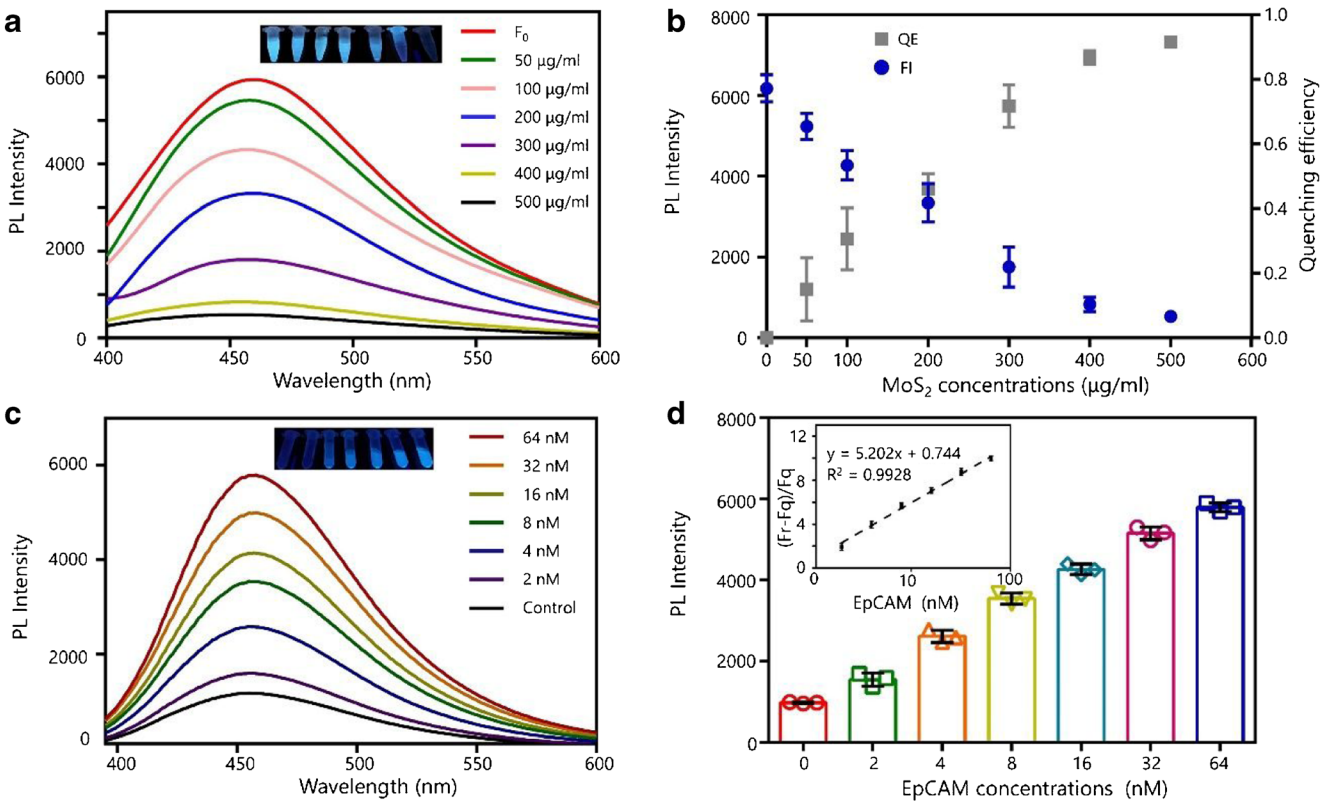

Fig. 4 **a** Fluorescence quenching spectra of the aptamer@Fe_3O_4@graphene quantum dot (GQD) complex with the addition of increasing concentrations of MoS_2 nanosheets, ranging from 50 to 500 μg/mL. The inset shows images of aptamer @Fe_3O_4@GQD@MoS_2 solutions under 365-nm UV irradiation. **b** Quenching efficiency (QE), (F_0-F_q)/F_0, and normalized photoluminescence (PL) intensity versus a series of MoS_2 nanosheet concentrations. **c** Fluorescence recovery spectra of the aptamer@Fe_3O_4@GQD@MoS_2-based sensing platform with the addition of target epithelial cell adhesion molecule (EpCAM) at various concentrations from 2 to 64 nM. The inset shows images of aptamer@Fe_3O_4@GQDs@MoS_2 solutions under 365-nm UV irradiation. **d** The recovered peak fluorescence signal versus a series of concentrations of the target EpCAM. The fitting logarithmic curve shown in the inset is that between the relative peak fluorescence signal and the EpCAM concentration. FI fluorescence intensity

After we had confirmed the ability of MoS_2 nanosheets to quench GQDs, EpCAM was detected with the aptamer@Fe_3O_4@GQD@MoS_2 sensing platform. The aptamer@Fe_3O_4@GQD@MoS_2-based nanocomposites were prepared with MoS_2 nanosheets at a concentration of 500 μg/mL. The initial quenching fluorescent signal can be reduced to a minimum and the highest (91.2%) quenching efficiency, for optimal sensor performance. Some preliminary experiments on the incubation time for EpCAM with nanocomposites were performed. The results showed that the fluorescence was restored to the maximum value after incubation for 1 h at room temperature (Fig. S9). Fluorescence recovery was quantified by our recording the PL spectra of aptamer@Fe_3O_4@GQD@MoS_2 complexes incubated with EpCAM for about 1 h. The average PL spectrum of aptamer@Fe_3O_4@GQD@MoS_2 complexes with increasing target EpCAM concentration is shown in Fig. 4c. When the concentration of the target EpCAM increased, the PL intensity of GQDs gradually increased. The maximum change in the PL signal between two adjacent spectral curves appears near 457 nm. Accordingly, the PL recovery signal was analyzed according to the signal of the spectral peak. Stronger affinity interaction between aptamers and target EpCAM leads to the aptamer@Fe_3O_4@GQD complex disengaging from the MoS_2 nanosheet surface, resulting in fluorescence recovery. With increasing distance between the donor GQDs and acceptor MoS_2 nanosheet, the NSET effect disappears, and the fluorescence signal is restored.

The PL signal of the nanobiosensor with different EpCAM concentrations is shown in Fig. 4d. The fluorescence recovery of the nanobiosensor was further analyzed. The relative recovery was calculated by $(F_r\text{-}F_q)/F_q$, where F_r is the recovered fluorescence intensity after addition of the target EpCAM and F_q is the fluorescence intensity of the aptamer@Fe_3O_4@GQD@MoS_2 complexes assayed after quenching. We used the equation $y = 5.202x + 0.744$ ($R^2 = 0.9928$) to obtain a linear relationship between the relative fluorescence signal recovery and the logarithm of the concentration, where y represents the relative recovery of the fluorescence peak signal (Fig. 4d, inset). On the basis of blank signals plus three times the standard derivation, the LOD for EpCAM detection was calculated to be 1.19 nM. The current method is primarily based on the use of anti-EpCAM antibodies. It is expensive and unstable for sensory detection. On the basis of our nanobiosensors, aptamers may be a cheap and stable platform for cancer biomarker detection.

Cell labeling by aptamer@Fe_3O_4@GQD complexes and detection of tumor cells

Firstly, the specificity of the aptamer@Fe_3O_4@GQD complexes for EpCAM was evaluated. The biosensor was tested for the same concentration of 64 nM EpCAM, bovine serum albumin (BSA), and immunoglobulin G (IgG). For better comparison, the PL signal of ultrapure water was used to normalize all measured PL signals. The other experimental conditions were the same as previously described. For BSA and IgG there was no significant fluorescence recovery signal, showing that the method can specifically detect EpCAM (Fig. 5a). The results also show that this detection method has excellent specificity for detection of EpCAM. This was consistent with previous research results [28].

Secondly, to prove the feasibility of our nanosensor to detect true cancer cells, a panel of cell lines, including two derived from tumors, the EpCAM-overexpressing hepatocellular carcinoma Hep G2 and low-EpCAM-expressing lung cancer A549 cells lines, and one derived from noncancerous tissues, the human epithelial kidney HEK293 (EpCAM-nonexpressing) cell line, were used as the target. The toxicity of aptamer@Fe_3O_4@GQD@MoS_2 complexes was first assessed. Aptamer@Fe_3O_4@GQD@MoS_2 complexes were added to a series of cells at increasing concentrations. The viability of the cells was determined 24 h later. The results presented in Fig. 5a reveal that aptamer@Fe_3O_4@GQD@MoS_2 complexes did not exhibit obvious toxicity at concentrations up to 100 μg/mL.

Thirdly, aptamer@Fe_3O_4@GQD@MoS_2 composites, at 200 mg/mL, were incubated with Hep G2, A549, and HEK293 cells (concentration 1.0×10^5 cells per milliliter), for 15 min, 2 h, and 6 h. After 15 min incubation, no obvious blue fluorescence was observed in HEK293 cells, whereas blue-fluorescence-labeled Hep G2 and A549 cells were clearly found, because a stronger bond between tumor cells and the aptamer leads to the detachment of the aptamer@Fe_3O_4@GQD complex from MoS_2 nanosheets and subsequent binding to tumor cells (Fig. 5b). Furthermore, the specificity of the aptamer@Fe_3O_4@GQD complex for EpCAM was enhanced by the nanocomposite conjugation with the tumor cells, which quickly labeled the tumor cells within 15 min. Meanwhile, a comparison of bare GQDs with aptamer@Fe_3O_4 @GQD complexes incubated with tumor cells revealed that after 2 h, the control (bare GQDs) still showed no obvious blue fluorescence (Fig. S6), but after 6 h incubation, because of endocytosis, the control showed blue fluorescence. The CellSearch platform captures only EpCAM-positive CTCs, and does not work for low-EpCAM-expressing and EpCAM-negative CTCs [33]. The experimental results in this study show that the detection system can achieve better detection of tumor cells (both low-EpCAM-expressing and EpCAM-overexpressing cells) and greatly reduces the detection time.

Fourthly, after determination of good specificity of the nanocomposite, we designed a method for tumor cell detection and enrichment. As shown in Fig. 5c, tumor cells were mixed with HEK293 negative control cells. After 15 min incubation, blue-fluorescence-labeled Hep G2 and A549 cells were clearly observed, while the control cells were not observed. These results once again prove the potential of this nanosensor for the detection of EpCAM-expressing cancer cells.

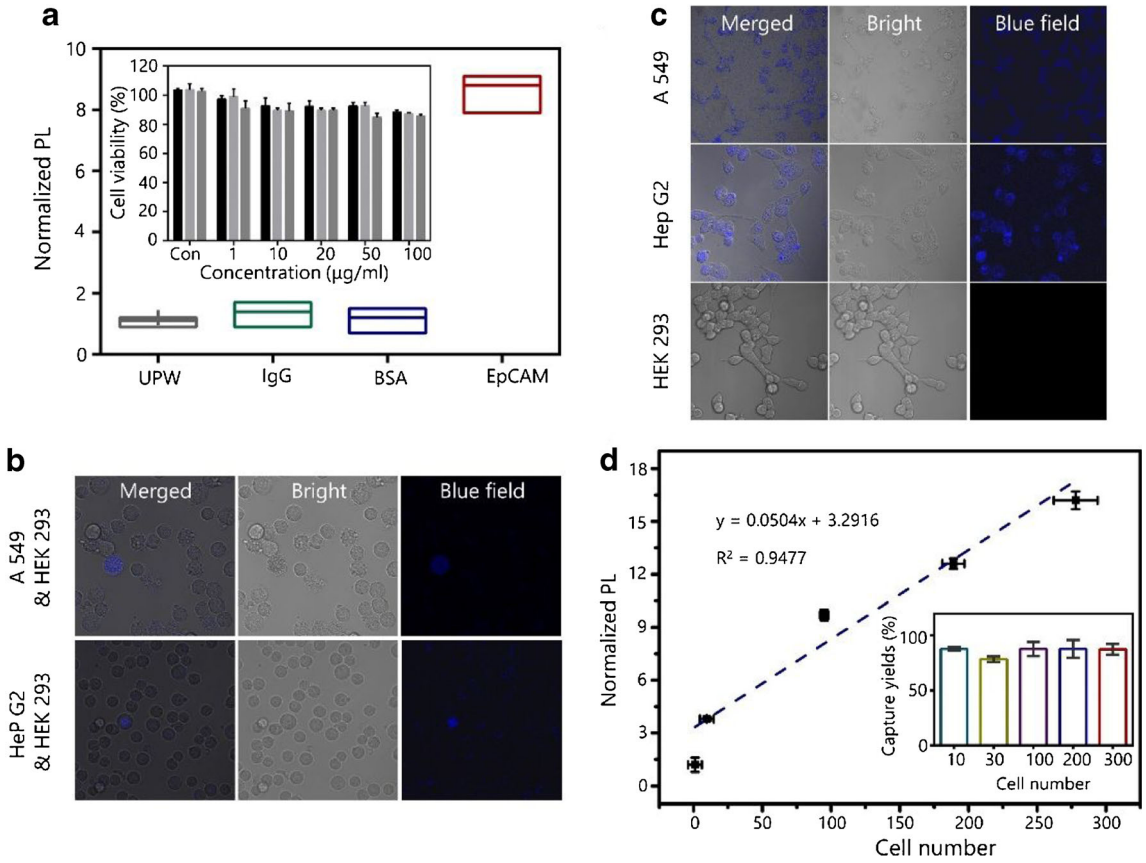

Fig. 5 **a** Specificity evaluation of the nanobiosensor with bovine serum albumin (BSA) and immunoglobulin G (IgG) as controls and toxicity (inset) of aptamer@Fe_3O_4@GQDs@MoS_2 complexes. **b** Detection of tumor cells (A549 and Hep G2) and negative control cells (HEK293) after incubation with the aptamer@Fe_3O_4@GQDs@MoS_2 composite for 15 min: representative confocal microscopy images of the indicated cells in merged (left), bright (middle), and blue (right) field. **c** Specific recognition of tumor cells (A549 and Hep G2 cells) by aptamer@Fe_3O_4@GQD@MoS_2 nanoprobes: confocal microscopy images of tumor cells (A549 and Hep G2 cells) in merged (left), bright (middle), and blue (right) field after incubation with aptamer@Fe_3O_4@GQD@MoS_2 complexes for 15 min. **d** The relationship between photoluminescence (PL) intensity and the number of cells captured by magnetic separation. The inset shows cell capture efficiencies of 10, 30, 100, 200, and 300 Hep G2 cells isolated by magnetic separation. Ulter-pure water (UPW)

Finally, the free nanoparticles were removed by washing. They were then isolated with a magnet. This allows the capture of positive cancer cells from a large number of negative cell pools. We estimated the number of positive tumor cells in the test sample by calculating the PL signal of GQDs (Fig. 5d). Different amounts of Hep G2 cells in 500 μL PBS were captured with aptamer@Fe_3O_4@GQD complexes. They were then separated with a magnet, and then the number of cells captured was counted under a microscope. It is worth noting that the cell capture efficiency of all samples reached approximately 80–90% (Fig. 5d, inset). This is 30% higher than with the one-step method involving magnetic nanoparticle CTCs modified with folic acid (Table S2) [34]. Further, the number of cells captured has a good linear relationship with the detected fluorescence values. This allowed us to calculate the number of CTCs captured by scaling the fluorescence value (Fig. 5d). With the increase in the number of cells found, the PL signal shows an increasing trend. Finally, the effect of Fe_3O_4 magnetic separation can effectively reduce interference from nonspecific signals from the negative cells (Fig. 5b). This promotes the aptamer-specific recognition of cells expressing EpCAM. In particular, in the presence of a large number of EpCAM non-expressing cells, the detection sensitivity can be improved. Therefore, this method has a high cell capture efficiency and causes no notable damage to the captured tumor cells. These advantages are beneficial for detecting and separating CTCs.

To test the effectiveness of our new strategy for detecting CTCs in real samples, 0.5 mL of healthy whole blood donated by healthy volunteers was used to simulate the blood of cancer patients by our adding different numbers of Hep G2 cells. Blood samples were incubated sequentially with magnetic fluorescent nanocomposites and subjected to magnetic separation, followed by measurement of the PL signal of the separated samples. As expected, as the number of tumor cells present in the sample increased, the fluorescence signal

showed a gradually increasing trend (Fig. S7). In summary, the method in the case of a lot of negative cells or whole blood is sensitive in detecting tumor cells. Further, the captured cells can be separated for further analysis, which is very important for future CTC studies.

Conclusions

In this work, we developed novel N,S/GQDs by using a facile approach. The resulting GQDs emit bright and stable blue luminescence in solution under single-wavelength UV excitation (λ= 340 nm). Additionally, we developed biosensors based on a new NSET aptamer@Fe_3O_4@GQD and MoS_2 nanosheet pair for the detection of EpCAM. An NSET test was successfully established for EpCAM detection; the linear range was between 2 and 64 nM, and the LOD was 1.19 nM. Because of the presence of aptamers, this nanobiosensor can quickly (15 min) and specifically identify and detect tumor cells (both low-EpCAM-expressing and EpCAM-overexpressing cells). In addition, we found that the application of magnetic separation of tumor cells was not only effective but also that in EpCAM-nonexpressing cells eliminates nonspecific aspects of cell signals, which may be a major issue restricting the detection sensitivity toward CTCs. Finally, we achieved high-sensitivity detection of as few as ten tumor cells in whole blood. Further, it is possible to easily separate the captured cells for further experimental study. This method may be a promising, sensitive, and convenient tumor cell detection and separation technique. It has high specificity and sensitivity and has great potential for early diagnosis and prognosis of cancer.

Acknowledgements This work was supported by the National Research Program of China (201513006, 31371768, 2016YFD0401204), the Postgraduate Research & Practice Innovation Program of Jiangsu Province (KYCX17_1413), the Collaborative Innovation Center for Food Safety and Quality Control, the Priority Academic Development Program of Jiangsu Higher Education Institutions, and the Agricultural science and technology innovation projects of Shanxi province, China (2015NY002).

Compliance with ethical standards

This study was approved by the Institute of Jiangnan University Medical Ethics Committee, and the investigation was performed according to the ethical guidelines in document no. JNUMEC-201801008, October 2018.

Informed consent Informed consent was obtained from all individual participants included in the study. All blood samples were obtained from healthy volunteers.

Conflict of interest The authors declare that they have no competing interests.

References

1. Nothacker M, Duda V, Hahn M, Warm M, Degenhardt F, Madjar H, et al. Early detection of breast cancer: benefits and risks of supplemental breast ultrasound in asymptomatic women with mammographically dense breast tissue. A systematic review. BMC Cancer. 2009;9(1):335.
2. Nguyen QT, Tsien RY. Fluorescence-guided surgery with live molecular navigation—a new cutting edge. Nat Rev Cancer. 2013;13(9):653–62.
3. Gorges TM, Pantel K. Circulating tumor cells as therapy-related biomarkers in cancer patients. Cancer Immunol Immun. 2013;62(5):931–9.
4. Poste G, Fidler IJ. The pathogenesis of cancer metastasis. Nature. 1980;283(5743):139–46.
5. Allard WJ, Matera J, Miller MC, Repollet M, Connelly MC, Rao C, et al. Tumor cells circulate in the peripheral blood of all major carcinomas but not in healthy subjects or patients with nonmalignant diseases. Clin Cancer Res. 2004;10(20):6897–904.
6. O'Connell CL, Nooney R, Mcdonagh C. Cyanine5-doped silica nanoparticles as ultra-bright immunospecific labels for model circulating tumour cells in flow cytometry and microscopy. Biosens Bioelectron. 2017;91:190–8.
7. Kalinich M, Bhan I, Kwan TT, Miyamoto DT, Javaid S, LiCausi JA, et al. An RNA-based signature enables high specificity detection of circulating tumor cells in hepatocellular carcinoma. Proc Natl Acad Sci U S A. 2017:201617032.
8. Gastl G, Spizzo G, Obrist P, Dünser M, Mikuz G. Ep-CAM overexpression in breast cancer as a predictor of survival. Lancet. 2000;356(9246):1981–2.
9. Varga M, Obrist P, Schneeberger S, Mühlmann G, Felgel-Farnholz C, Fong D, et al. Overexpression of epithelial cell adhesion molecule antigen in gallbladder carcinoma is an independent marker for poor survival. Clin Cancer Res. 2004;10(9):3131–6.
10. Fong D, Steurer M, Obrist P, Barbieri V, Margreiter R, Amberger A, et al. Ep-CAM expression in pancreatic and ampullary carcinomas: frequency and prognostic relevance. J Clin Pathol. 2008;61(1):31–5.
11. Liu L-L, Fu D, Ma Y, Shen X-Z. The power and the promise of liver cancer stem cell markers. Stem Cells Dev. 2011;20(12):2023–30.
12. Shi J, Lyu J, Tian F, Yang M. A fluorescence turn-on biosensor based on graphene quantum dots (GQDs) and molybdenum disulfide (MoS_2) nanosheets for epithelial cell adhesion molecule (EpCAM) detection. Biosens Bioelectron. 2017;93:182–8.
13. Armstrong A, Eck SL. EpCAM: a new therapeutic target for an old cancer antigen. Cancer Biol Ther. 2003;2(4):320–5.
14. Tan W, Donovan MJ, Jiang J. Aptamers from cell-based selection for bioanalytical applications. Chem Rev. 2013;113(4):2842–62.
15. Jayanthi VSA, Das AB, Saxena U. Recent advances in biosensor development for the detection of cancer biomarkers. Biosens Bioelectron. 2016.
16. Zhao B, Wu P, Zhang H, Cai C. Designing activatable aptamer probes for simultaneous detection of multiple tumor-related proteins in living cancer cells. Biosens Bioelectron. 2015;68:763–70.
17. Zhang C-Y, Yeh H-C, Kuroki MT, Wang T-H. Single-quantum-dot-based DNA nanosensor. Nat Mater. 2005;4(11):826–31.
18. Ye WW, Tsang MK, Liu X, Yang M, Hao J. Upconversion luminescence resonance energy transfer (LRET)-based biosensor for rapid and ultrasensitive detection of avian influenza virus H7 subtype. Small. 2014;10(12):2390–7.

19. Cai Z, Li F, Wu P, Ji L, Zhang H, Cai C, et al. Synthesis of nitrogen-doped graphene quantum dots at low temperature for electrochemical sensing trinitrotoluene. Anal Chem. 2015;87(23):11803–11.
20. Chen Z, Liang R, Guo X, Liang J, Deng Q, Li M, et al. Simultaneous quantitation of cytokeratin-19 fragment and carcinoembryonic antigen in human serum via quantum dot-doped nanoparticles. Biosens Bioelectron. 2017;91:60–5.
21. Yang Y, Liu Q, Liu Y, Cui J, Liu H, Wang P, et al. A novel label-free electrochemical immunosensor based on functionalized nitrogen-doped graphene quantum dots for carcinoembryonic antigen detection. Biosens Bioelectron. 2017;90:31–8.
22. Fan Z, Li S, Yuan F, Fan L. Fluorescent graphene quantum dots for biosensing and bioimaging. RSC Adv. 2015;5(25):19773–89.
23. Wang Y, Meng Y, Wang S, Li C, Shi W, Chen J, et al. Direct solvent-derived polymer-coated nitrogen-doped carbon nanodots with high water solubility for targeted fluorescence imaging of glioma. Small. 2015;11(29):3575–81.
24. Tan X, Li Y, Li X, Zhou S, Fan L, Yang S. Electrochemical synthesis of small-sized red fluorescent graphene quantum dots as a bioimaging platform. Chem Commun. 2015;51(13):2544–6.
25. Guo R, Zhou S, Li Y, Li X, Fan L, Voelcker NH. Rhodamine-functionalized graphene quantum dots for detection of $Fe3^{+}$ in cancer stem cells. 2015.
26. Shi J, Chan C, Pang Y, Ye W, Tian F, Lyu J, et al. A fluorescence resonance energy transfer (FRET) biosensor based on graphene quantum dots (GQDs) and gold nanoparticles (AuNPs) for the detection of mecA gene sequence of Staphylococcus aureus. Biosens Bioelectron. 2015;67:595–600.
27. Ge J, Lan M, Zhou B, Liu W, Guo L, Wang H, et al. A graphene quantum dot photodynamic therapy agent with high singlet oxygen generation. Nat Commun. 2014;5.
28. Song Y, Zhu Z, An Y, Zhang W, Zhang H, Liu D, et al. Selection of DNA aptamers against epithelial cell adhesion molecule for cancer cell imaging and circulating tumor cell capture. Anal Chem. 2013;85(8):4141–9.
29. Fan Z, Zhou S, Garcia C, Fan L, Zhou J. pH-Responsive fluorescent graphene quantum dots for fluorescence-guided cancer surgery and diagnosis. Nanoscale. 2017;9(15):4928.
30. Tang L, Ji R, Li X, Bai G, Liu CP, Hao J, et al. Deep ultraviolet to near-infrared emission and photoresponse in layered n-doped graphene quantum dots. ACS Nano. 2014;8(6):6312–20.
31. Peng J, Gao W, Gupta BK, Liu Z, Romero-Aburto R, Ge L, et al. Graphene quantum dots derived from carbon fibers. Nano Lett. 2012;12(2):844–9.
32. Zhou J, Yang Y, Zhang C-Y. A low-temperature solid-phase method to synthesize highly fluorescent carbon nitride dots with tunable emission. Chem Commun. 2013;49(77):8605–7.
33. Vila A, Abal M, Muinelo-Romay L, Rodriguez-Abreu C, Rivas J, López-López R, et al. EGFR-based immunoisolation as a recovery target for low-EpCAM CTC subpopulation. PLoS One. 2016;11(10):e0163705.
34. Nie L, Li F, Huang X, Aguilar ZP, Wang YA, Xiong Y, et al. Folic acid targeting for efficient isolation and detection of ovarian cancer CTCs from human whole blood based on two-step binding strategy. ACS Appl Mater Interfaces. 2018.